Articles
doi.org/10.1002/batt.202000246

Chemistry Europe
European Chemical Societies Publishing

Special Collection

Enabling Mg-Based Ionic Liquid Electrolytes for Hybrid Dual-Ion Capacitors

Paul Meister,[a] Verena Küpers,[a] Martin Kolek,[a] Johannes Kasnatscheew,[a] Sebastian Pohlmann,[a] Martin Winter,*[a, b] and Tobias Placke*[a]

We report on the reversible (de)intercalation of $TFSI^-$ anions from a Mg-based ionic liquid electrolyte, $Mg(TFSI)_2$ in $Pyr_{14}TFSI$, in graphite || activated carbon hybrid dual-ion capacitor (DIC) cells. The role of different pseudo reference electrodes (PREs) including Ag-wire and Li metal is discussed regarding the comparability of different battery cells. We show that an Ag-wire PRE is not suitable for the designated purpose, while the use of a Li metal PRE results in high reproducibility. Mg-based DIC cells are compared with cells based on pure $Pyr_{14}TFSI$ and LiTFSI-$Pyr_{14}TFSI$ electrolytes, and with graphite || Li metal dual-ion cells employing LiTFSI-$Pyr_{14}TFSI$. At 5.2 V *vs.* $Li|Li^+$, Mg-containing DIC cells reveal an improved performance compared to Li-based cells, *i.e.*, higher capacity (87 *vs.* 85 $mAh\,g^{-1}$) and higher Coulombic efficiency (98 *vs.* 96 %). These results may pave the way to further studies and performance improvements of Mg-based batteries and to hybrid DIC chemistries with other cations, especially multi-valent ones.

1. Introduction

Beside state-of-the-art lithium (Li) ion batteries (LIBs), various novel battery concepts, such as sodium- (Na-), potassium- (K-), calcium- (Ca-), or magnesium- (Mg)-based batteries, got significant attention in the recent decade.[1] Even though a high theoretical energy density is predicted, many of these alternative battery technologies suffer from a reduced practical energy density compared to LIBs and are therefore mainly of interest for specific applications, such as stationary energy storage.[1d,e,2] However, research and development of these battery technologies is motivated by promises for improved sustainability aspects, including higher material abundance, use of renewable resources, a claimed improved CO_2 footprint, and better recyclability.[3] The dual-ion battery (DIB) technology, and dual-graphite (DGB), or dual-carbon batteries (DCB) as its special forms, have gained much attention as emerging electrochemical energy storage technology, as they are considered to have benefits in terms of material and element abundance, ease of processing, recycling, cost, and safety compared to other rechargeable batteries.[4]

Unlike the "classical" LIB cell chemistry, which is based on a cationic ion-transfer principle, DIB cells are based on the simultaneous storage of cations and anions at the negative (anode) and positive electrode (cathode), respectively.[4a,5] In case of DGB cells, the storage mechanism is based on the simultaneous (de-)intercalation of cations/anions into (or from) the graphite anode/cathode.[6] The electrolyte serves as reservoir for cations and anions and is part of the active materials, thus, having a huge impact on the theoretical and practical battery cell energy density.[2a,4a] Various cell chemistries and electrolyte approaches have been reported for DIB cells, which can be categorized according to their active cationic (*e.g.*, Li^+, Na^+, K^+, Zn^{2+}, Mg^{2+})[5,7] and anionic species (*e.g.*, PF_6^-, BF_4^-, $AlCl_4^-$, imide anions),[8] to their electrolyte solvents (*e.g.*, highly concentrated electrolytes,[6c,9] ionic liquid electrolytes,[5,7a,8a,10] hybrid aqueous/non-aqueous electrolytes,[11] or water-in-(bi)salt electrolytes)[12] and their active host anode and cathode materials.[4a]

A major focus for development of advanced DIB cells is on the design and analysis of novel electrolyte concepts and components (cation, anion, and solvent(s)) to improve cell performance and energy density. The electrolyte has a significant impact on the specific discharge capacity, the reversibility and cycling stability with respect to anion (de-) intercalation into/from the graphite cathode.[4a,5,8a,d,13] As anion intercalation starts at relatively high potentials (*e.g.*, ≈4.4 V *vs.* $Li|Li^+$ for $TFSI^-$), electrolytes offering a high oxidative stability are mandatory to achieve a high reversibility, which is reflected by a high Coulombic efficiency (C_{Eff}) of at least >99 %. Electrolyte decomposition must be avoided/diminished at such high potentials. The most promising electrolyte concepts

[a] Dr. P. Meister, V. Küpers, M. Kolek, Dr. J. Kasnatscheew, Dr. S. Pohlmann, Prof. Dr. M. Winter, Dr. T. Placke
University of Münster
MEET Battery Research Center
Institute of Physical Chemistry
Corrensstr. 46, 48149 Münster, Germany
E-mail: tobias.placke@uni-muenster.de
m.winter@fz-juelich.de
[b] Prof. Dr. M. Winter
Helmholtz Institute Münster
IEK-12, Forschungszentrum Jülich GmbH
Corrensstr. 46, 48149 Münster, Germany

Supporting information for this article is available on the WWW under https://doi.org/10.1002/batt.202000246

Special Collection An invited contribution to a joint Special Collection between ChemElectroChem and Batteries & Supercaps dedicated to research Beyond Lithium-Ion Batteries

reported so far include ionic liquid (IL) electrolytes,[5,7a,8a,10] highly concentrated electrolytes[6c,7h,9] as well as electrolytes offering a sufficient "high-voltage" stability.[6d] DIB cells also show a high energy efficiency (>92%),[7c,9a] a key performance parameter, which is often neglected.[14]

Magnesium bis(trifluoromethanesulfonyl) imide ($Mg(TFSI)_2$) can be a highly appealing electrolyte salt for DIB cells, due to the higher abundance of Mg and the potentially lower costs of the salt.[3] It offers the possibility to intercalate two $TFSI^-$ anions (instead of one in case of Li^+, Na^+ or K^+) in the graphite cathode, while one Mg^{2+} is stored at the anode. Thus, Mg-based salts have advantages compared to the more abundant Na-salts[7b,c] or K-salts,[6c,7d,e] considering the molecular weight of the electrolyte salt per unit charge involved in the redox reaction. For S || Li metal and S || Mg metal cells, the role of different cations like Li^+ and Mg^{2+} on the electrolyte has been addressed previously.[15] The influence of complex solution structures of Mg-based electrolytes on the electrodeposition and -dissolution behavior at the Mg anode, however, reveals an intricate interplay at the anode's interface.[16] Even though reversible electrodeposition and -dissolution of Mg^{2+} ions in IL-based electrolytes has been reported by some groups,[17] the results could not be reproduced by others,[18] which might be addressed by suitable IL-functionalization.[19] One major challenge of Mg-based batteries, *i.e.*, the lacking compatibility of conventional battery electrolyte-containing anions (*e.g.*, BF_4^-, PF_6^-, or $TFSI^-$) with Mg metal anodes was referred to the formation of passivating layers at Mg metal which do not allow sufficient Mg^{2+} transport.[20] These inorganic and organic Mg salt-containing surface films were formed spontaneously and during cycling by reactions between the active metal and the components of the solution[20b] and they did not act like a solid electrolyte interphase (SEI),[21] but were electronically and ionically insulating, thus, the electrode was truly "passivated".[20b] In addition to Mg metal, also alternative anodes such as insertion-type or alloying-type anodes were reported for Mg-ion batteries (MIBs). Especially insertion-type anodes might be compatible with a broader range of electrolyte compositions, but their often sluggish diffusion of Mg^{2+} and resulting low rate capability remain challenging.[22] The first published Mg-based DIB cell, shown by *Lei et al.*, for example combines expanded graphite with an organic Mg^{2+}-intercalating anode material (3,4,9,10-perylenetetracarboxylic diimide) to enable $TFSI^-$-intercalation using $Mg(TFSI)_2$ in $Pyr_{14}TFSI$.[7g] Recently, *Yang et al.* reported on a Mg-based DIB cell using expanded graphite as cathode and Ti-doped niobium pentoxide nanoflakes as fast kinetics anode.[7i]

Due to the unfavorable surface and interphase chemistry of Mg metal, we propose a hybrid system comprising of an activated carbon (AC) anode and a graphitic carbon cathode in this contribution, *i.e.*, a Mg metal-free cell. In such a system, the Mg^{2+} and Pyr_{14}^+ cations are physically adsorbed/de-adsorbed at the highly porous anode, whereby a reversible electrodeposition/-dissolution of the cations is not necessary. In contrast to that, the $TFSI^-$ anions are stored at the cathode by means of electrochemical intercalation/de-intercalation processes. We thereby exhibit a transition-metal free, potentially cheap alternative battery type beyond Li chemistry, which may also have advantages in terms of specific energy compared to the Na- and K-counterparts as explained above. A schematic illustration of the working principle is given in Figure 1.

An analogous system, using an AC anode and a graphitic carbon cathode was already presented as "megalo-capacitance capacitor" by *Yoshio et al.* in 2006.[23] However, to highlight the underlying energy storage mechanism, we would like to use another term for cells using this type of electrode setup and charge/discharge mechanisms. In analogy to Li ion capacitors (LICs),[24] in which, *e.g.*, a Li ion-intercalation anode and an AC cathode are used, hence, combining two different storage mechanisms ((de-)intercalation and adsorption/desorption in the double layer), the term "hybrid dual-ion capacitor" (DIC) will be used here.

The focus of this work was to study the intercalation behavior of $TFSI^-$ anions into the positive electrode from a Mg-based IL electrolyte under various cycling and cell operation conditions. To avoid issues of the complex surface chemistry of Mg metal in a three-electrode setup, alternative pseudo reference electrodes including silver-wire (Ag) and Li metal were evaluated. In addition, the intercalation and de-intercalation processes are discussed based on differential capacity profiles and compared with Li-based DIB cells.

2. Results and Discussion

2.1. Performance Studies in a Half-Cell Setup Using Ag-Wire as Pseudo-Reference Electrode

The specific discharge capacity of two different graphite || AC DIC cells using an Ag-wire as pseudo reference electrode (PRE) is illustrated in Figure 2a and c. In these cells, the graphite WE potential was controlled *via* the Ag-wire PRE, while AC served

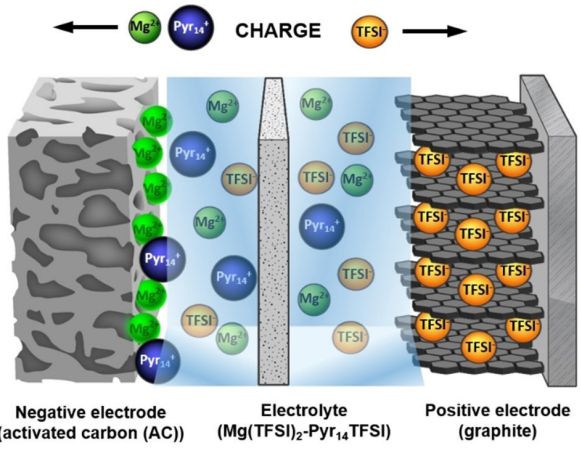

Figure 1. Simplified illustration of the working principle of a hybrid dual-ion capacitor. During charge, Mg^{2+} and Pyr_{14}^+ cations are stored *via* a physical adsorption process at the porous activated carbon (AC) negative electrode, while the $TFSI^-$ anions are intercalated into the graphite positive electrode because of a Faradaic reaction. During discharge, the reversible processes take place, hence, the ions are released back into the electrolyte.

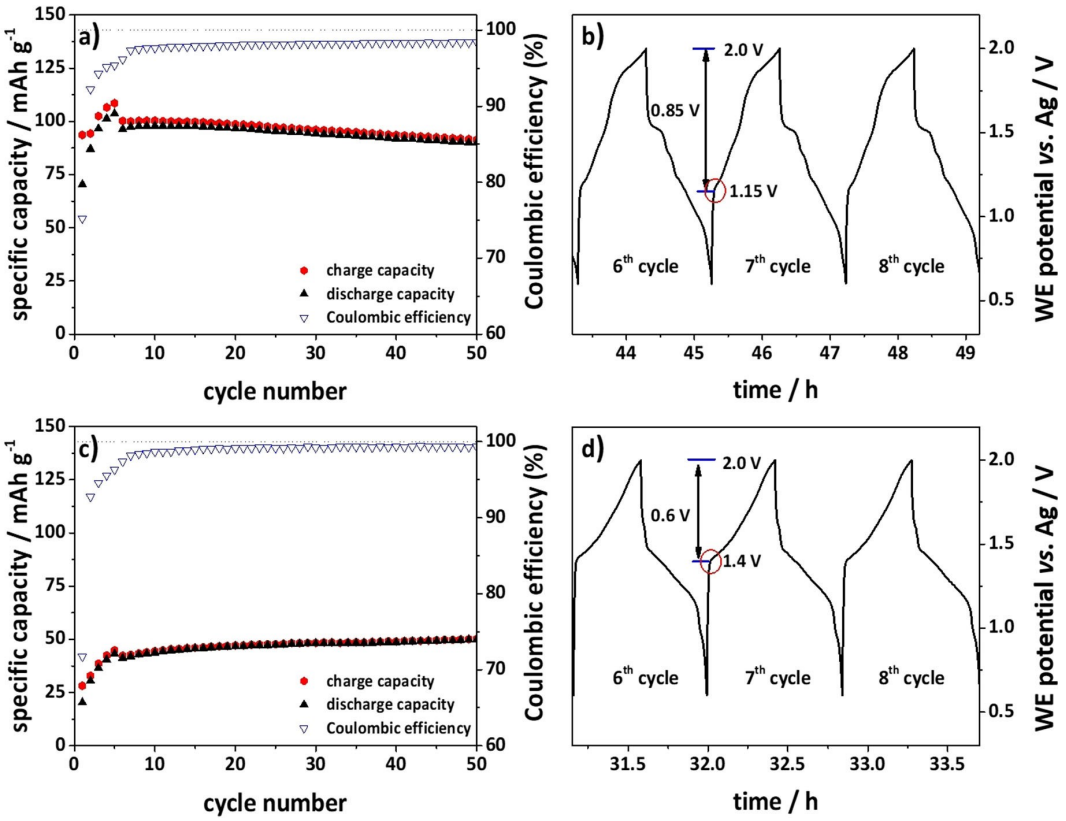

Figure 2. a, c) Specific charge and discharge capacities as well as Coulombic efficiency *vs.* cycle number and b, d) the corresponding WE potential *vs.* time profiles of two different graphite || AC dual-ion capacitor cells during constant current charge/discharge cycling. Cell setup: A; potential range: 0.6-2.0 V *vs.* Ag; 50 mA g^{-1} (cycle 1–5) and 100 mA g^{-1} (from cycle 6); Electrolyte: 0.3 M $Mg(TFSI)_2$ in $Pyr_{14}TFSI$.

as CE (cell setup A, Figure 8a). At first sight, a different course of the specific capacity is observed in both cells even though the same conditions were set for the constant current cycling, indicating a poor reproducibility. For both cells, an increase in Coulombic efficiency (C_{Eff}) and capacity is obtained during the first cycles, which was ascribed to an enhanced wetting of the composite electrodes by the viscous IL-based electrolyte as well as a kind of "formation/activation" process caused by an increase in the interlayer gap distance between the graphene layers during anion intercalation.[7a,25] The first cell (Figure 2a) exhibited a discharge capacity of ≈98 mAh g^{-1} in the 6th cycle, which decreased to ≈90 mAh g^{-1} in cycle 50. In contrast, the second cell (Figure 2c) provided only a discharge capacity of ≈41 mAh g^{-1} in the 6th cycle, which increased to ≈50 mAh g^{-1} in the 50th cycle. However, the C_{Eff} in the first cell leveled off at ≈98%, while it exceeded 99% in the second cell. Hence, the increased discharge capacity of the first cell was achieved at the expense of a reduced C_{Eff}, which is well-known from our previous studies on DIB cells and can most likely be ascribed to enhanced electrolyte decomposition and self-discharge reactions.[5,6f,7a,c,10a]

To identify the origin of the significant deviation between both cells, the potential profiles of the graphite working electrodes (WEs) were studied in detail. The onset potential for anion uptake in the first cell is located at ≈1.15 V *vs.* Ag (Figure 2b). In consideration of the upper cut-off potential of 2.0 V *vs.* Ag, an anion intercalation range of 0.85 V is obtained. By comparison, the onset potential of the second cell is shifted to 1.4 V *vs.* Ag (Figure 2d). In consequence, the anion intercalation voltage range of the second cell is reduced to 0.6 V compared to the first cell. Based on the staging mechanism of $TFSI^-$-intercalation into graphite, the specific capacity and consequently the amount of intercalated anions strongly depend on the upper cut-off potential. The $TFSI^-$ intercalation capacity in graphite||Li metal cells almost doubles, when the cut-off potential is increased from 5.0 V *vs.* $Li|Li^+$ (50 mAh g^{-1}) to 5.2 V *vs.* $Li|Li^+$ (85 mAh g^{-1}) or 5.3 V *vs.* $Li|Li^+$ (97 mAh g^{-1}), while C_{Eff} decreases from >99% to 96% or even to 90%.[5] The deviation between both cells can therefore be referred to the difference in the intercalation voltage range.[5,25]

For the investigation of room temperature ILs, the use of PREs, such as Ag- or platinum (Pt-)-wires, has often been reported.[26] However, the utilization of these PREs is also accompanied by several challenges. In general, these types of PREs operate by the presence of different surface compounds. The composition of these surface groups might change if they dissolve in or react with the electrolyte. *Snook et al.* reported an average standard deviation of 100 mV within five runs of a cyclic voltammetry experiment for a solution of 5 mM ferrocene in $Pyr_{14}TFSI$.[27] Other groups also reported significant potential shifts of several hundred millivolts for common Ag or Pt PREs.[28] Taking this observation into account, the strong

deviation of the cycling performance of both cells should originate from different shifts of the potential of the Ag-wire PRE over time. In other words, with reference to the same absolute potential scale, the potential of the Ag-wire in the first cell was located at a ≈0.25 V more positive potential than the one of the second cell. This in turn means that the graphite electrode in the first cell is exposed to a higher upper cut-off potential than in the second cell. For this reason, higher discharge capacities and lower C_{Eff} were obtained in the first cell.

2.2. Performance Studies in a Full-Cell Setup

To circumvent the above-mentioned issues related to the use of PREs, the first approach in this work was to change the cell setup to a full-cell setup (B, Figure 8b). Here, the cell voltage was controlled between the AC negative electrode (anode) and graphite positive electrode (cathode). Furthermore, Li metal was used as the reference electrode to monitor, but not to control, the single electrode potentials by means of auxiliary cables.[29] Figure 3a illustrates the specific capacity and the C_{Eff} for Mg-based graphite || AC DIC cells. Starting from ≈14 mAh g^{-1} in the 1st cycle, the discharge capacity rose to ≈35 mAh g^{-1} in the 50th cycle. The standard deviation (SD) accounted for ≈0.1 to 0.2 mAh g^{-1}. Due to this low SD value, it was not explicitly included in the graphical illustration in Figure 3a. The cells exhibited a C_{Eff} of ≈65% in the 1st cycle, which rose to 92% in the 2nd cycle. In the subsequent cycles, the C_{Eff} leveled off at high values and reached 99% after 27 cycles. The relative standard deviation (RSD) of the C_{Eff} accounted for 0.3% in the 1st cycle and decreased to a level below 0.1% within the next few cycles.

As the upper cut-off potential of the cathode directly influences the capacity of DIB cells,[5,7a] the cell voltage as well as the anode and cathode potential were studied in detail. Figure 3b displays the course of the cell voltage (black line), the potential of the AC anode (thin blue line) and the potential of the graphite cathode (thick blue line). The anode potential showed the typical triangular shape of AC electrodes with a low potential drop (≈11 mV). Generally, values ranging from 2.90 V to 3.04 V *vs.* Li|Li$^+$ were recorded for the anode potential during cycling. The course of the cathode potential profiles pointed at an onset potential for anion uptake (indicated by a red dashed line) of ≈4.4 V *vs.* Li|Li$^+$. Considering a maximum graphite electrode potential of 4.94 V *vs.* Li|Li$^+$, a total intercalation voltage range of 0.54 V is attained. For DIB cells using Li metal as anode and a mixture of LiTFSI-Pyr$_{14}$TFSI as electrolyte, the average discharge capacity ranges between 42 to 50 mAh g^{-1} at upper cut-off potentials of 4.9 V and 5.0 V *vs.* Li|Li$^+$.[5] As an onset potential for anion uptake of 4.4 V *vs.* Li|Li$^+$ was found, these charging end potentials can be translated to an intercalation range of 0.5 V to 0.6 V.[5] Therefore, the observed capacity of ≈35 mAh g^{-1} in

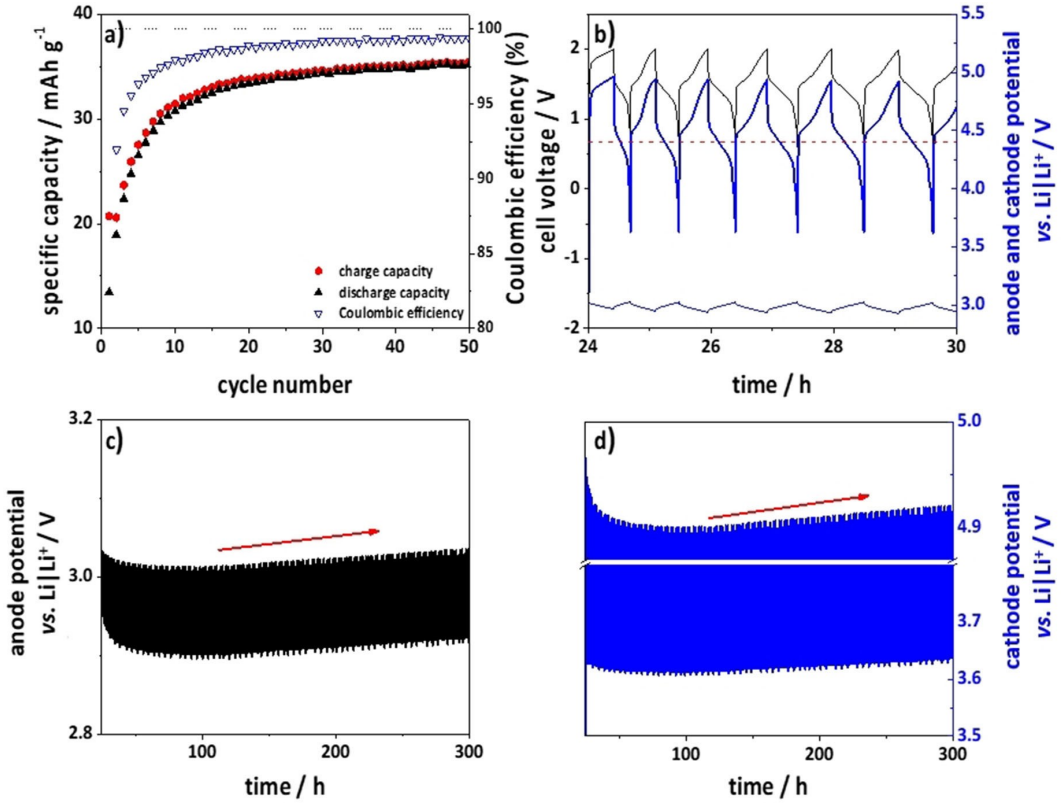

Figure 3. a) Specific charge and discharge capacities as well as Coulombic efficiency *vs.* cycle number of the first 50 cycles as well as b) representative cell voltage (black line), anode potential (thin blue line) and cathode potential (thick blue line) *vs.* time profiles; long-term evolution of c) the anode and d) the cathode potential. The measurements were performed using cell setup B. Cell voltage: 0.6–2.0 V; 50 mA g^{-1}; Electrolyte: 0.3 M Mg(TFSI)$_2$ in Pyr$_{14}$TFSI.

the Mg-based DIC is lower than expected from the Li-based DIB cell. The long-term course of the anode and cathode potentials of the graphite || AC DIC cells is shown in Figure 3c and d, respectively. As indicated by the red arrows, an increase of ≈6 mV in the upper cut-off potential of both the graphite cathode and the AC anode is recorded during cycling. Hence, the discharge capacity, which is directly affected by the upper cut-off potential of the cathode, also increases upon cycling.

2.3. Performance Studies in a Half-Cell Setup Using Li Metal as Pseudo-Reference Electrode

For a better comparison of the cycling performance of DICs and in order to avoid a drift of the upper cut-off potential of the WE/cathode,[29] the graphite WE potential was further controlled *via* a Li metal PRE ("half-cell" setup C, Figure 8c). Figure 4 illustrates the discharge capacity and C_{Eff} of DIC cells cycled at different upper cut-off potentials varying from 4.8 V to 5.2 V *vs.* Li|Li$^+$. The corresponding average values of cycle 20 to 40 as well as the standard deviations are summarized in Table 1. In general, a behavior typical for anion intercalation like in DIB cells was found, *i.e.*, an increase in the upper cut-off potential yielded in higher discharge capacities and reduced C_{Eff}.[5]

At an upper cut-off potential of 4.8 V *vs.* Li|Li$^+$, a discharge capacity of only ≈25 mAh g^{-1} was determined, while at 5.2 V *vs.* Li|Li$^+$ a significant increase to ≈87 mAh g^{-1} was observed (Figure 4). The highest value for the C_{Eff} accounted for ≈99.0% at 4.8 V and 4.9 V *vs.* Li|Li$^+$, respectively. The lowest average C_{Eff} of ≈97.5% was determined at 5.1 V *vs.* Li|Li$^+$, but at this potential the average of the standard deviation also showed the highest value (Table 1). The reduction of the C_{Eff} with increasing upper cut-off potential can be correlated with enhanced parasitic side reactions, such as decomposition of intercalated anions or increased self-discharge.[4a]

The cell voltage profiles (50th cycle) of the Mg-based DIC cells cycled to different upper WE cut-off potentials are shown in Figure S1a, and the corresponding graphite WE potential profiles are illustrated in Figure S1b. Even though the time was normalized from 0 to 1, to allow for a better comparison of the voltage/WE potential profiles, the appearance of an increasing number of plateau regions during charge and discharge with increasing upper WE cut-off potential is still clearly visible. An even better comparison of the (de-)intercalation potential regions in dependence of the upper cut-off potential can be observed from the differential capacity (dQ/dV) profiles (Figure 5). A broad range for TFSI$^-$ intercalation can be identified, *i.e.*, ranging from ≈4.4 V to 5.2 V *vs.* Li|Li$^+$. There are two major peaks for anion uptake at ≈4.5 V *vs.* Li|Li$^+$ and at >5.0 V *vs.* Li|Li$^+$. In addition, another peak appears at ≈4.7 V *vs.* Li|Li$^+$ for the cells operated at an upper cut-off potential ≥5.1 V, suggesting differences in the intercalation mechanism. In general, these peaks correspond to the staging mechanism for TFSI$^-$ (de-)intercalation, as shown by *in situ* XRD studies in previous publications.[7d,30] For de-intercalation, several potential peaks and potential ranges can be observed: All DIC cells show TFSI$^-$ de-intercalation at ≈4.0 V *vs.* Li|Li$^+$ and in the range of ≈4.2 to 4.5 V *vs.* Li|Li$^+$.

The DIC cells operated at 5.0 V *vs.* Li|Li$^+$ or even higher cut-off potentials feature additional de-intercalation peaks at ≈4.6 V and ≈4.8 V *vs.* Li|Li$^+$, which can be clearly correlated to the

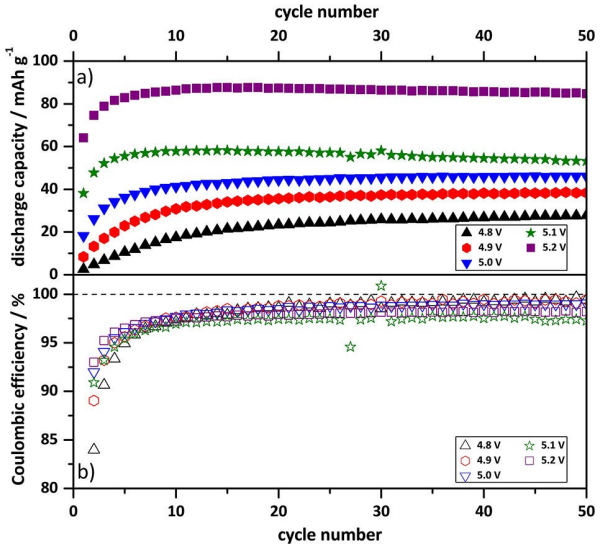

Figure 4. a) Specific discharge capacities and b) Coulombic efficiencies *vs.* cycle number of graphite || AC DIC cells (cell setup C) at a charge/discharge current of 50 mA g^{-1} of the first 50 cycles. Potential range: 3.4 V to 4.8–5.2 V *vs.* Li|Li$^+$; 50 mA g^{-1}; Electrolyte: 0.3 M Mg(TFSI)$_2$ in Pyr$_{14}$TFSI.

Table 1. Correlation of the upper cut-off potential to the average values of the discharge capacity and Coulombic efficiency (including standard deviation) for graphite || AC DIC cells (cell setup C) in the range of cycle 20 to 40 of the constant current charge/discharge cycling experiments.

Upper cut-off potential *vs.* Li|Li$^+$ [V]	Average discharge capacity [mAh g^{-1}]	Average Coulombic efficiency [%]
4.8	24.9 ± 1.6	99.0 ± 0.1
4.9	36.8 ± 1.2	99.0 ± 0.2
5.0	45.3 ± 0.7	98.7 ± 0.1
5.1	56.4 ± 1.3	97.5 ± 0.7
5.2	86.6 ± 1.3	98.0 ± 0.1

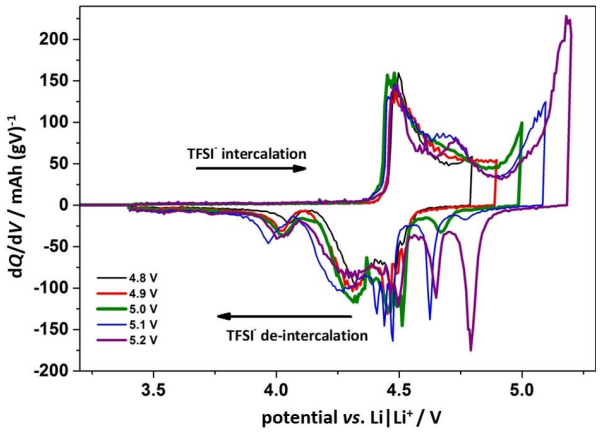

Figure 5. Comparison of specific differential capacity profiles (dQ/dV) of graphite || AC DIC cells (cell setup C using a Li metal PRE), during constant current charge/discharge cycling. Potential range: 3.4 V to 4.8 -5.2 V *vs.* Li|Li$^+$; 50 mA g^{-1}; Electrolyte: 0.3 M Mg(TFSI)$_2$ in Pyr$_{14}$TFSI.

additional capacity gain obtained for anion intercalation above ≈5.0 V *vs.* Li|Li$^+$. The observed trends for TFSI$^-$ anion (de-) intercalation from Mg(TFSI)$_2$-Pyr$_{14}$TFSI correlate well with the previous findings for LiTFSI-Pyr$_{14}$TFSI electrolytes.[5,30–31]

2.4. Evaluation and Comparison of DIC Cells and Li-based DIB Cells

In the following, Mg-based graphite || AC DIC cells will be compared to Li-based DIC cells using 0.3 M LiTFSI-Pyr$_{14}$TFSI as electrolyte and to DIC cells using the pure Pyr$_{14}$TFSI electrolyte. In addition, the specific capacity, and potential ranges for (de-) intercalation are compared to those of graphite || Li metal DIB cells. For the Mg- and Li-based DIC cells, no significant difference is observed in terms of their specific capacity during charge/discharge cycling (Figure 6) as well as in terms of their (de-)intercalation potentials, as illustrated by the overlay of the differential capacity profiles (50th cycle) for TFSI$^-$ anion uptake/release into/from graphite (Figure 7 and Figure S2). Furthermore, there is also almost no difference compared to the

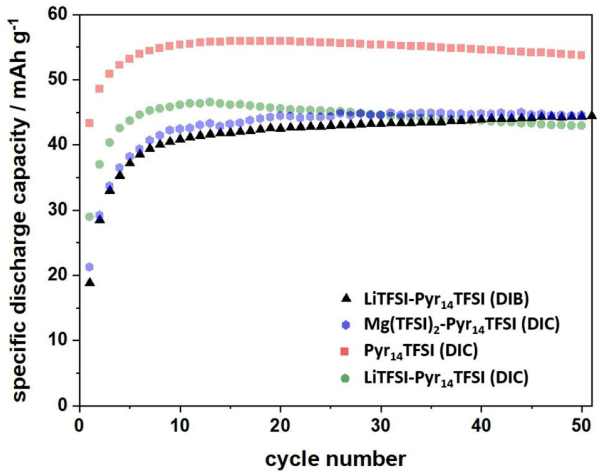

Figure 6. Specific discharge capacities *vs.* cycle number of graphite || AC DIC cells using either Pyr$_{14}$TFSI (red), 0.3 M LiTFSI in Pyr$_{14}$TFSI (green) or 0.3 M Mg(TFSI)$_2$ in Pyr$_{14}$TFSI (blue) as electrolyte. In addition, a graphite || Li metal DIB cell (0.3 M LiTFSI in Pyr$_{14}$TFSI; black) is shown. Charge/discharge current: 50 mA g^{-1}; Potential range: 3.4 V to 5.0 V *vs.* Li|Li$^+$.

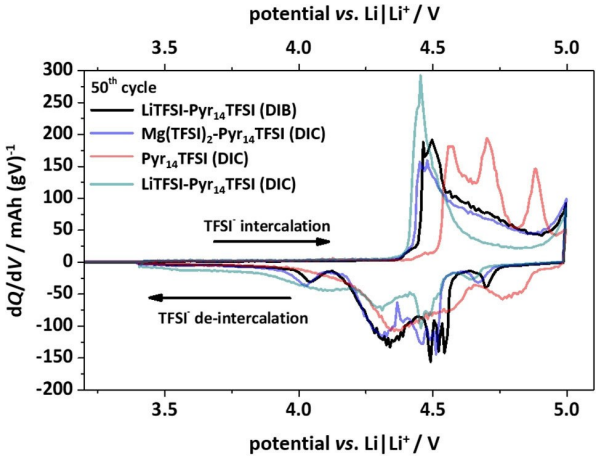

Figure 7. Comparison of specific differential capacity *vs.* potential profiles (d*Q*/d*V*) of graphite || Li metal DIB cells (cell setup C using a Li metal RE and CE) and graphite || AC DIC cells (cell setup C using a Li metal RE/PRE), during constant current charge/discharge cycling with a specific current of 50 mA g^{-1}. In each case, the 50th cycle is illustrated. Either 0.3 M LiTFSI in Pyr$_{14}$TFSI (Li-based DIB (black) and DIC (green)), 0.3 M Mg(TFSI)$_2$ in Pyr$_{14}$TFSI (Mg-based DIC (blue)) or the pure IL Pyr$_{14}$TFSI (Pyr$_{14}$TFSI-DIC (red)) were used as electrolyte.

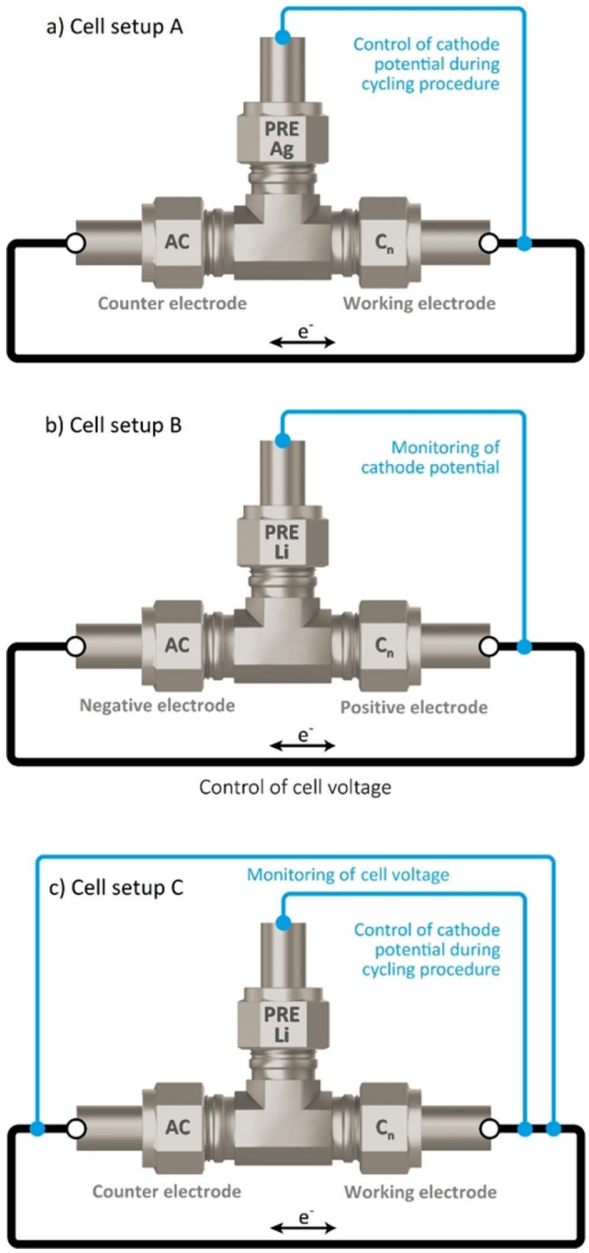

Figure 8. a) Cell setup A (half-cell setup): Graphite WE potential is controlled between 0.6 V and 2.0 V *vs.* Ag *via* the Ag-wire PRE, while cell voltage and AC CE potential will vary (not controlled). b) Cell setup B (full-cell setup): Cell voltage is controlled between 0.6 and 2.0 V, while the potential of the graphite positive electrode is only monitored *via* the Li metal PRE. The potential of the AC negative electrode is calculated as difference between positive electrode potential and cell voltage. c) Cell setup C (half-cell setup): Graphite WE potential is controlled between 3.4 V and 4.8–5.2 V *vs.* Li|Li$^+$ *via* the Li metal PRE, and cell voltage is monitored using auxiliary cables.

graphite || Li metal DIB cells based on the LiTFSI-Pyr_{14}TFSI electrolyte with respect to capacity and (de-)intercalation potentials. The three cell systems (Li-based DIB cells, Li-based and Mg-based DIC cells) showed very similar onset potentials of ≈4.39 V to 4.41 V *vs.* $Li|Li^+$ for anion intercalation (threshold value 20 $mAh\,g^{-1}$ V^{-1}). During the anodic scan, two peaks associated with anion intercalation and stage formation[30] with two maxima located at ≈4.4 to 4.5 V and 5.0 V *vs.* $Li|Li^+$, respectively, were found for all three systems, as already discussed above for the Mg-based DIC cells (Figure 5). Regarding the cathodic scan, three main regions were detected for anion de-intercalation for all three cell systems (Figure 7), *i.e.*, at ≈4.0 V *vs.* $Li|Li^+$ and in the range of ≈4.2 to 4.5 V *vs.* $Li|Li^+$ and at ≈4.6 V *vs.* $Li|Li^+$.

In contrast to the Li- and Mg-based cells, the use of the pure Pyr_{14}TFSI electrolyte in graphite || AC DIC cells results in significant changes of the (de-)intercalation potentials (Figure 7) as well as an improved specific capacity (increase of ≈15 $mAh\,g^{-1}$) at 5.0 V (Figure 6 and Figure S2). The onset potential for anion intercalation is shifted to a significantly higher value ≈4.5 V *vs.* $Li|Li^+$, while three major intercalation regions are seen at ≈4.6 V, 4.7 V and 4.9 V *vs.* $Li|Li^+$. The increased capacity also results in an additional de-intercalation peak at ≈4.8 V *vs.* $Li|Li^+$ (Figure 7). The improved capacity in these graphite || AC DIC cells can most likely be associated with either improved kinetics for anion storage and an improved storage capacity/capacitance of Pyr_{14}^+ cations at the AC electrode compared other cations such as Li^+ or Mg^{2+}.[32] In general, the specific capacitance of highly porous carbon electrodes (*e.g.*, AC) significantly depends on the ratio of pore size and the size of the (solvated) ions, as shown in previous works.[33] Here, we find the following trend in terms of double layer storage capacitance: $Pyr_{14}^+ > Pyr_{14}^+/Mg^{2+} > Pyr_{14}^+/Li^+$ (see also Figure S2). Thus, the electrolyte based on pure Pyr_{14}TFSI also delivers an enhanced capacity in the hybrid DIC system, due to the improved storage of Pyr_{14}^+ cations at the AC anode/counter electrode.

Nevertheless, it must be considered that the use of the Li^+ and Mg^{2+} cations will be beneficial in terms of capacity and stability when changing to intercalation/insertion-based anode materials due to their smaller size. Furthermore, it is known that the compatibility of Pyr_{14}TFSI with graphite negative electrodes is rather poor, as there is no effective SEI formation when not applying additional electrolyte additives.[34]

Further electrochemical results on the voltage efficiency and energy efficiency for the four different DIC and DIB cells are shown in the supporting information (Figure S3 and Figure S4).

The graphite || Li metal DIB cells display the highest voltage and energy efficiencies (>90%) from all systems.

With regard to C_{Eff}, a level above or equal to 99% was maintained up to 5.0 V *vs.* $Li|Li^+$ for the Li-based DIB cells,[5] while the Mg-based DIC cells provided such a high C_{Eff} only up to 4.9 V *vs.* $Li|Li^+$. The reduced oxidative stability at higher potentials might be related to the lower purity of $Mg(TFSI)_2$ (99.5%) as compared to LiTFSI (99.95%), which will result in increased electrolyte decomposition reactions or even enhanced aluminum (Al) current collector dissolution.[35] These parasitic side reactions consume additional charge, thus, leading to a reduction of the C_{Eff}. However, the reduced discharge capacity in the Mg-based DIC cells might also be related to a different intercalation/de-intercalation behavior of the $TFSI^-$ anions compared to DIC cells using pure Pyr_{14}TFSI. Possible factors that could influence the uptake of the anions into the graphite structure are properties of the electrolyte, such as ion pair formation or the presence of different charge species $[M(TFSI)_x]^{y-}$ (with $M = Li^+$, Mg^{2+}, *etc.*).[8a,18b] Furthermore, due to the interplay of the anion uptake into the graphite positive electrode and the electrodeposition/adsorption/intercalation of cations on/into the negative electrode, overpotentials at the anode side will also have an impact on the anion uptake.[7c]

In this work, we pointed out that $TFSI^-$ anion intercalation into a graphite cathode from a Mg-based ionic liquid electrolyte can offer high specific capacities of up to ≈86 $mAh\,g^{-1}$ within a graphite || AC hybrid DIC. Future works should focus on the combination of a graphite cathode and suitable insertion- or alloying-type anodes for Mg^{2+} storage for further capacity and energy improvements.

3. Conclusions

The reversible (de-)intercalation of $TFSI^-$ anions from a Mg-based ionic liquid electrolyte was demonstrated for the first time in a hybrid dual-ion capacitor (DIC) system. It has been shown that Ag-wire as pseudo reference electrode (PRE) is not suitable for the designated purpose within this experimental setup. Instead, Li metal has been applied as PRE in two different ways. In the first setup, it has been used to monitor the cathode potential. The results showed an increase of the anode and cathode potential upon cycling. As the cathode potential has an influence on the anion uptake and release, the Li metal reference electrode was also used to control the potential of the positive electrode to improve the comparability of different cells. Generally, it can be stated that the application of Li metal as PRE resulted in reproducible cycling performance, whereas this was not observed in the case of the Ag-wire PRE.

For the cathode potential controlled DIC cells, where the cathode is the working electrode in a three-electrode set-up, a reasonably high capacity of ≈45 $mAh\,g^{-1}$ was obtained at 5.0 V *vs.* $Li|Li^+$ with a high Coulombic efficiency of ≈99%. Taking into account only the capacity of the 50th cycle, a slightly lower capacity (45 $mAh\,g^{-1}$ *vs.* 50 $mAh\,g^{-1}$) was attained for the DIC cells than for Li-based DIBs, while the Coulombic efficiency was still in the same range. The electrochemical performance at 5.2 V *vs.* $Li|Li^+$ revealed an even improved performance for the Mg-containing cells. Besides a higher capacity (87 $mAh\,g^{-1}$ *vs.* 85 $mAh\,g^{-1}$) also a higher Coulombic efficiency is gained (98% *vs.* 96%). These results may pave the way for further studies on the design of suitable cell setups and improvements of Mg-based storage devices and DICs using other cations than Mg.

Experimental Section

Electrode and electrolyte preparation

Electrode tapes for the positive electrode were composed of 90 wt.% KS6L graphite (Imerys Graphite & Carbon), 5 wt.% of conductive carbon black agent C-nergy™ Super C65 (Imerys Graphite & Carbon) and 5 wt.% of sodium carboxymethylcellulose (Na-CMC) as binder (Walocel CRT 2000 PPA 12, Dow Wolff Cellulosics) on an Al current collector. The preparation of the electrodes was conducted as reported previously.[5] The average mass loading of the graphite electrodes accounted for 2.5 ± 0.1 mg cm^{-2}.

The self-standing AC electrodes were composed of 85 wt.% DLC Super 30 (Norit), 10 wt.% of conductive carbon black agent C-nergy™ Super C65 (Imerys Graphite & Carbon) and 5 wt.% of polytetrafluoroethylene (PTFE) as binder (60 wt.% dispersion in H_2O, Sigma-Aldrich). At first, the binder was dissolved in de-ionized water. In total, a weight to volume ratio of 0.17 g mL^{-1} was used, hence, 1 g solid was added to 6 mL of water. Then, the proper amount of the conductive agent C-nergy™ Super C65 was added and the dispersion was homogenized by magnetic stirring for 1 hour. Subsequently, AC was added and the electrode paste was further homogenized for 1 hour. To remove excess water, the electrode paste was slowly heated up to 60 °C. Afterwards, the resulting paste was vigorously kneaded to increase its density. Thereafter, it was rolled into flat sheets with a thickness of ≈1 mm. Electrode discs with a diameter of 12 mm were punched out of the sheets. In the last step, the discs were dried for 12 hours at 80 °C, followed by an additional drying step at 180 °C at a reduced pressure of < 1 Pa for 20 hours. The AC electrodes were used in large excess in terms of capacity/capacitance to avoid any limitations for anion intercalation at the cathode.

A mixture of 0.3 M magnesium bis(trifluoromethanesulfonyl) imide ($Mg(TFSI)_2$, purity: 99.5 %, Solvionic) respectively 0.3 M lithium bis (trifluoromethanesulfonyl) imide (LiTFSI, purity: 99.95 %, Solvionic) in the IL *N*-butyl-*N*-methylpyrrolidinium bis(trifluoromethanesulfonyl) imide ($Pyr_{14}TFSI$, purity: 99.9 %, Solvionic) were utilized as electrolytes. Prior to use, the conductive salt as well as the IL were dried at 110 °C following a high vacuum drying procedure (< $1 \cdot 10^{-5}$ Pa). The water content of the dried IL was < 10 ppm, as determined by Karl-Fischer titration. The mixing as well as the storage of the electrolyte was carried out in an argon-filled glove box (MBraun) with water and oxygen contents below 1 ppm.

Electrochemical characterization

All electrochemical investigations were performed in lab-scale Swagelok-type T-cells with a three-electrode setup. Glass microfiber filters (Whatman, grade GF/D) were used as separator, which were soaked with 120 µL or 80 µL (reference electrode) of electrolyte. After cell assembly, the cells rested for 24 hours at room temperature to ensure a sufficient "wetting" of the electrodes by the viscous IL-based electrolyte. Three different cell setups were used in this work, further abbreviated as setup A (Figure 8a), setup B (Figure 8b) and setup C (Figure 8c). In setup A, which is a "half-cell" setup,[29] the graphite working electrode (WE) is cycled in a defined potential range vs. an Ag-wire (Alfa Aesar, purity: 99.9 %) as pseudo reference electrode (PRE), resulting in a varying (not controlled) anode potential and cell voltage. The cut-off potentials were set to 0.6 V and 2.0 V *vs.* Ag. Oversized AC-based electrodes were used as counter electrode (CE) in this setup. For constant current charge/discharge cycling, the specific current was set to 50 mA g^{-1} (based on graphite) for the first five cycles followed by 100 mA g^{-1} for subsequent cycling.

In the cell setups B and C, Li metal (Albemarle, battery grade) was used as PRE in combination with different cycling procedures. In setup B (Figure 8b), the cell voltage was controlled between 0.6 and 2.0 V, whereas the positive electrode potential was only monitored by means of the Li metal PRE with additional auxiliary cables (full-cell setup).[29] The corresponding negative electrode potential was calculated as difference between the positive electrode potential and the cell voltage. During charge/discharge, a specific current of 50 mA g^{-1} was applied for the measurements. As the positive electrode potential has a strong impact on the intercalation and de-intercalation of anions,[5] it must be controlled to achieve a maximum comparability of the different measurements. In this context, cell setup C (Figure 8c) was used, where the graphite WE potential was controlled *via* the Li metal PRE and the cell voltage was monitored using auxiliary cables (half-cell setup).[29] The cut-off potentials were adjusted to 3.4 V *vs.* Li | Li$^+$ and ranging from 4.8 V to 5.2 V *vs.* Li | Li$^+$ at a specific current of 50 mA g^{-1}.

Supporting information

Supporting information for this article is available on the WWW under https://doi.org/

Acknowledgments

The authors wish to thank the Federal Ministry of Education and Research (BMBF) for funding this work in the projects "Insider" (03EK3031A) within the "Förderinitiative Energiespeicher" and "MgMeAnS" (03XP0140). We also thank Andre Bar for graphical support. Open access funding enabled and organized by Projekt DEAL.

Conflict of Interest

The authors declare no conflict of interest.

Keywords: anion intercalation · dual-ion capacitor · hybrid capacitor · ionic liquid electrolyte · magnesium

[1] a) T. Placke, R. Kloepsch, S. Dühnen, M. Winter, *J. Solid State Electrochem.* **2017**, *21*, 1939–1964; b) T. Hosaka, K. Kubota, A. S. Hameed, S. Komaba, *Chem. Rev.* **2020**, *120*, 6358–6466; c) R. J. Gummow, G. Vamvounis, M. B. Kannan, Y. He, *Adv. Mater.* **2018**, *30*, 1801702; d) Y. Liang, H. Dong, D. Aurbach, Y. Yao, *Nat. Energy* **2020**, *5*, 646–656; e) Y. E. Durmus, H. Zhang, F. Baakes, G. Desmaizieres, H. Hayun, L. Yang, M. Kolek, V. Küpers, J. Janek, D. Mandler, S. Passerini, Y. Ein-Eli, *Adv. Energy Mater.* **2020**, *10*, 2000089; f) A. Ponrouch, J. Bitenc, R. Dominko, N. Lindahl, P. Johansson, M. R. Palacin, *Energy Storage Mater.* **2019**, *20*, 253–262; g) P. Bonnick, J. Muldoon, *Adv. Funct. Mater.* **2020**, *30*, 1910510.

[2] a) J. Betz, G. Bieker, P. Meister, T. Placke, M. Winter, R. Schmuch, *Adv. Energy Mater.* **2019**, *9*, 1803170; b) M. Winter, B. Barnett, K. Xu, *Chem. Rev.* **2018**, *118*, 11433–11456.

[3] S. Dühnen, J. Betz, M. Kolek, R. Schmuch, M. Winter, T. Placke, *Small Methods* **2020**, *4*, 2000039.

[4] a) T. Placke, A. Heckmann, R. Schmuch, P. Meister, K. Beltrop, M. Winter, *Joule* **2018**, *2*, 2528–2550; b) S. Chen, Q. Kuang, H. J. Fan, *Small* **2020**, *16*, 2002803; c) K. V. Kravchyk, M. V. Kovalenko, *Adv. Energy Mater.* **2019**, *9*, 1901749; d) M. Wang, Y. Tang, *Adv. Energy Mater.* **2018**, *8*, 1703320;

e) X. Zhou, Q. Liu, C. Jiang, B. Ji, X. Ji, Y. Tang, H.-M. Cheng, *Angew. Chem. Int. Ed.* **2020**, *59*, 3802–3832; f) I. A. Rodríguez-Pérez, X. Ji, *ACS Energy Lett.* **2017**, *2*, 1762–1770.
[5] T. Placke, O. Fromm, S. F. Lux, P. Bieker, S. Rothermel, H. W. Meyer, S. Passerini, M. Winter, *J. Electrochem. Soc.* **2012**, *159*, A1755-A1765.
[6] a) J. R. Dahn, J. A. Seel, *J. Electrochem. Soc.* **2000**, *147*, 899–901; b) B. Heidrich, A. Heckmann, K. Beltrop, M. Winter, T. Placke, *Energy Storage Mater.* **2019**, *21*, 414–426; c) P. Münster, A. Heckmann, R. Nölle, M. Winter, K. Beltrop, T. Placke, *Batteries Supercaps* **2019**, *2*, 992–1006; d) J. A. Read, A. V. Cresce, M. H. Ervin, K. Xu, *Energy Environ. Sci.* **2014**, *7*, 617–620; e) S. Rothermel, P. Meister, O. Fromm, J. Huesker, H. W. Meyer, M. Winter, T. Placke, *ECS Trans.* **2014**, *58*, 15–25; f) S. Rothermel, P. Meister, G. Schmuelling, O. Fromm, H. W. Meyer, S. Nowak, M. Winter, T. Placke, *Energy Environ. Sci.* **2014**, *7*, 3412–3423; g) A. Heckmann, O. Fromm, U. Rodehorst, P. Münster, M. Winter, T. Placke, *Carbon* **2018**, *131*, 201–212.
[7] a) T. Placke, P. Bieker, S. F. Lux, O. Fromm, H. W. Meyer, S. Passerini, M. Winter, *Z. Phys. Chem.* **2012**, *226*, 391–407; b) L. Fan, Q. Liu, S. Chen, Z. Xu, B. Lu, *Adv. Energy Mater.* **2017**, *7*, 1602778; c) P. Meister, O. Fromm, S. Rothermel, J. Kasnatscheew, M. Winter, T. Placke, *Electrochim. Acta* **2017**, *228*, 18–27; d) K. Beltrop, S. Beuker, A. Heckmann, M. Winter, T. Placke, *Energy Environ. Sci.* **2017**, *10*, 2090–2094; e) B. Ji, F. Zhang, X. Song, Y. Tang, *Adv. Mater.* **2017**, *29*, 1700519; f) Q. Guo, K.-i. Kim, H. Jiang, L. Zhang, C. Zhang, D. Yu, Q. Ni, X. Chang, T. Chen, H. Xia, X. Ji, *Adv. Funct. Mater.* **2020**, *30*, 2002825; g) X. Lei, Y. Zheng, F. Zhang, Y. Wang, Y. Tang, *Energy Storage Mater.* **2020**, *30*, 34–41; h) X. Li, X. Ou, Y. Tang, *Adv. Energy Mater.* **2020**, *10*, 2002567; i) R. Yang, F. Zhang, X. Lei, Y. Zheng, G. Zhao, Y. Tang, C.-S. Lee, *ACS Appl. Mater. Interfaces* **2020**, *12*, 47539–47547; j) A. Yu, Q. Pan, M. Zhang, D. Xie, Y. Tang, *Adv. Funct. Mater.* **2020**, *30*, 2001440.
[8] a) K. Beltrop, P. Meister, S. Klein, A. Heckmann, M. Grünebaum, H.-D. Wiemhöfer, M. Winter, T. Placke, *Electrochim. Acta* **2016**, *209*, 44–55; b) L. Zhang, D. Zhu, H. Wang, *J. Electrochem. Soc.* **2019**, *166*, A2654-A2659; c) L. Zhang, J. Li, Y. Huang, D. Zhu, H. Wang, *Langmuir* **2019**, *35*, 3972–3979; d) O. Fromm, P. Meister, X. Qi, S. Rothermel, J. Huesker, H. W. Meyer, M. Winter, T. Placke, *ECS Trans.* **2014**, *58*, 55–65.
[9] a) A. Heckmann, J. Thienenkamp, K. Beltrop, M. Winter, G. Brunklaus, T. Placke, *Electrochim. Acta* **2018**, *260*, 514–525; b) L. Xiang, X. Ou, X. Wang, Z. Zhou, X. Li, Y. Tang, *Angew. Chem. Int. Ed.* **2020**, *132*, 18080–18086; c) S. Miyoshi, H. Nagano, T. Fukuda, T. Kurihara, M. Watanabe, S. Ida, T. Ishihara, *J. Electrochem. Soc.* **2016**, *163*, A1206-A1213.
[10] a) P. Meister, V. Siozios, J. Reiter, S. Klamor, S. Rothermel, O. Fromm, H. W. Meyer, M. Winter, T. Placke, *Electrochim. Acta* **2014**, *130*, 625–633; b) K. Beltrop, J. C. Madrid Madrid, P. Meister, A. Heckmann, M. Winter, T. Akbay, T. Ishihara, T. Placke, *J. Power Sources* **2020**, *469*, 228397.
[11] a) J. M. Wrogemann, S. Künne, A. Heckmann, I. A. Rodríguez-Pérez, V. Siozios, B. Yan, J. Li, M. Winter, K. Beltrop, T. Placke, *Adv. Energy Mater.* **2020**, *10*, 1902709; b) J. Zhu, Y. Xu, Y. Fu, D. Xiao, Y. Li, L. Liu, Y. Wang, Q. Zhang, J. Li, X. Yan, *Small* **2020**, *16*, 1905838.
[12] a) I. A. Rodríguez-Pérez, L. Zhang, J. M. Wrogemann, D. M. Driscoll, M. L. Sushko, K. S. Han, J. L. Fulton, M. H. Engelhard, M. Balasubramanian, V. V. Viswanathan, V. Murugesan, X. Li, D. Reed, V. Sprenkle, M. Winter, T. Placke, *Adv. Energy Mater.* **2020**, *10*, 2001256; b) H. Zhang, X. Liu, B. Qin, S. Passerini, *J. Power Sources* **2020**, *449*, 227594.
[13] X. Jiang, L. Luo, F. Zhong, X. Feng, W. Chen, X. Ai, H. Yang, Y. Cao, *ChemElectroChem* **2019**, *6*, 2615–2626.
[14] P. Meister, H. Jia, J. Li, R. Klöpsch, M. Winter, T. Placke, *Chem. Mater.* **2016**, *28*, 7203–7217.
[15] a) G. Bieker, J. Wellmann, M. Kolek, K. Jalkanen, M. Winter, P. M. Bieker, *Phys. Chem. Chem. Phys.* **2017**, *19*, 11152–11162; b) G. Bieker, D. Diddens, M. Kolek, O. Borodin, M. Winter, P. Bieker, K. Jalkanen, *J. Phys. Chem. C* **2018**, *122*, 21770–21783.
[16] G. Bieker, M. Salama, M. Kolek, Y. Gofer, P. Bieker, D. Aurbach, M. Winter, *ACS Appl. Mater. Interfaces* **2019**, *11*, 24057–24066.
[17] a) Y. NuLi, J. Yang, J. Wang, J. Xu, P. Wang, *Electrochem. Solid-State Lett.* **2005**, *8*, C166-C169; b) Y. NuLi, J. Yang, R. Wu, *Electrochem. Commun.* **2005**, *7*, 1105–1110.
[18] a) N. Amir, Y. Vestfrid, O. Chusid, Y. Gofer, D. Aurbach, *J. Power Sources* **2007**, *174*, 1234–1240; b) G. A. Giffin, A. Moretti, S. Jeong, S. Passerini, *J. Phys. Chem. C* **2014**, *118*, 9966–9973; c) G. A. Giffin, *J. Mater. Chem. A* **2016**, *4*, 13378–13389; d) G. Vardar, A. E. S. Sleightholme, J. Naruse, H. Hiramatsu, D. J. Siegel, C. W. Monroe, *ACS Appl. Mater. Interfaces* **2014**, *6*, 18033–18039; e) G. T. Cheek, W. E. O'Grady, S. Z. El Abedin, E. M. Moustafa, F. Endres, *J. Electrochem. Soc.* **2008**, *155*, D91-D95.
[19] X. Gao, A. Mariani, S. Jeong, X. Liu, X. Dou, M. Ding, A. Moretti, S. Passerini, *J. Power Sources* **2019**, *423*, 52–59.
[20] a) N. Singh, T. S. Arthur, C. Ling, M. Matsui, F. Mizuno, *Chem. Commun.* **2013**, *49*, 149–151; b) D. Aurbach, I. Weissman, Y. Gofer, E. Levi, *Chem. Rec.* **2003**, *3*, 61–73.
[21] M. Winter, *Z. Phys. Chem.* **2009**, *223*, 1395–1406.
[22] K. Jayasayee, R. Berthelot, K. C. Lethesh, E. M. Sheridan, in *Magnesium Batteries: Research and Applications* (Ed.: M. Fichtner), The Royal Society of Chemistry, **2020**, pp. 114–141.
[23] M. Yoshio, H. Nakamura, H. Y. Wang, *Electrochem. Solid-State Lett.* **2006**, *9*, A561-A563.
[24] a) K. Naoi, P. Simon, *Electrochem. Soc. Interface* **2008**, *17*, 34–37; b) M. Schroeder, S. Menne, J. Segalini, D. Saurel, M. Casas-Cabanas, S. Passerini, M. Winter, A. Balducci, *J. Power Sources* **2014**, *266*, 250–258; c) M. Schroeder, M. Winter, S. Passerini, A. Balducci, *J. Power Sources* **2013**, *238*, 388–394; d) M. Schroeder, M. Winter, S. Passerini, A. Balducci, *J. Electrochem. Soc.* **2012**, *159*, A1240-A1245.
[25] T. Placke, O. Fromm, S. Rothermel, G. Schmuelling, P. Meister, H. W. Meyer, S. Passerini, M. Winter, *ECS Trans.* **2013**, *50*, 59–68.
[26] a) B. Huber, B. Roling, *Electrochim. Acta* **2011**, *56*, 6569–6572; b) D. Weingarth, A. Foelske-Schmitz, A. Wokaun, R. Kötz, *Electrochem. Commun.* **2012**, *18*, 116–118; c) P. A. Z. Suarez, V. M. Selbach, J. E. L. Dullius, S. Einloft, C. M. S. Piatnicki, D. S. Azambuja, R. F. de Souza, J. Dupont, *Electrochim. Acta* **1997**, *42*, 2533–2535; d) R. G. Evans, O. V. Klymenko, C. Hardacre, K. R. Seddon, R. G. Compton, *J. Electroanal. Chem.* **2003**, *556*, 179–188.
[27] G. A. Snook, A. S. Best, A. G. Pandolfo, A. F. Hollenkamp, *Electrochem. Commun.* **2006**, *8*, 1405–1411.
[28] a) A. M. Bond, P. A. Lay, *J. Electroanal. Interfacial Electrochem.* **1986**, *199*, 285–295; b) A. Ponrouch, C. Frontera, F. Barde, M. R. Palacin, *Nat. Mater.* **2016**, *15*, 169–173.
[29] R. Nölle, K. Beltrop, F. Holtstiege, J. Kasnatscheew, T. Placke, M. Winter, *Mater. Today* **2020**, *32*, 131–146.
[30] G. Schmuelling, T. Placke, R. Kloepsch, O. Fromm, H. W. Meyer, S. Passerini, M. Winter, *J. Power Sources* **2013**, *239*, 563–571.
[31] A. Heckmann, P. Meister, L.-Y. Kuo, M. Winter, P. Kaghazchi, T. Placke, *Electrochim. Acta* **2018**, *284*, 669–680.
[32] S. Pohlmann, T. Olyschlaeger, P. Goodrich, J. A. Vicente, J. Jacquemin, A. Balducci, *J. Power Sources* **2015**, *273*, 931–936.
[33] a) S. Pohlmann, R.-S. Kuehnel, T. A. Centeno, A. Balducci, *ChemElectroChem* **2014**, *1*, 1301–1311; b) S. Pohlmann, B. Lobato, T. A. Centeno, A. Balducci, *Phys. Chem. Chem. Phys.* **2013**, *15*, 17287–17294.
[34] M. Nadhérna, J. Reiter, J. Moskon, R. Dominko, *J. Power Sources* **2011**, *196*, 7700–7706.
[35] P. Meister, X. Qi, R. Kloepsch, E. Krämer, B. Streipert, M. Winter, T. Placke, *ChemSusChem* **2017**, *10*, 804–814.

Manuscript received: October 18, 2020
Revised manuscript received: November 18, 2020
Accepted manuscript online: November 19, 2020
Version of record online: December 10, 2020